NEUROSCIENCE

Noncanonical function of an autophagy protein prevents spontaneous Alzheimer's disease

Bradlee L. Heckmann[1]*, Brett J. W. Teubner[2], Emilio Boada-Romero[1], Bart Tummers[1], Clifford Guy[1], Patrick Fitzgerald[1], Ulrike Mayer[3], Simon Carding[4], Stanislav S. Zakharenko[2], Thomas Wileman[4,5], Douglas R. Green[1]*

Noncanonical functions of autophagy proteins have been implicated in neurodegenerative conditions, including Alzheimer's disease (AD). The WD domain of the autophagy protein Atg16L is dispensable for canonical autophagy but required for its noncanonical functions. Two-year-old mice lacking this domain presented with robust β-amyloid (Aβ) pathology, tau hyperphosphorylation, reactive microgliosis, pervasive neurodegeneration, and severe behavioral and memory deficiencies, consistent with human disease. Mechanistically, we found this WD domain was required for the recycling of Aβ receptors in primary microglia. Pharmacologic suppression of neuroinflammation reversed established memory impairment and markers of disease pathology in this novel AD model. Therefore, loss of the Atg16L WD domain drives spontaneous AD in mice, and inhibition of neuroinflammation is a potential therapeutic approach for treating neurodegeneration and memory loss. A decline in expression of ATG16L in the brains of human patients with AD suggests the possibility that a similar mechanism may contribute in human disease.

INTRODUCTION

Roles for autophagy in suppressing the pathogenesis of neurodegenerative conditions, including Alzheimer's disease (AD) (*1*, *2*) and a decline in expression of components of the autophagy machinery with age and in the AD brain (*3*–*6*), highlight the importance of this process in homeostasis. However, many autophagy proteins perform functions distinct from canonical autophagy (*7*, *8*). For example, the WD domain of the autophagy protein Atg16L is required for the lipidation of the microtubule-associated protein 1A/1B light chain 3B (LC3) at single membranes, while it is dispensable for the Atg16L-mediated LC3 lipidation in canonical autophagy (*9*, *10*). Autophagy and pathways that use the autophagy machinery are known to function in the regulation of amyloid generation, neuronal homeostasis, and β-amyloid (Aβ) clearance (*11*–*14*). It has been well established that Aβ clearance occurs through vesicular trafficking processes characterized by single membranes, including endocytosis in microglial cells (*14*–*19*). A direct link between these processes and the lipidation of LC3 on these single membranes, events that require components of the autophagy machinery, has been demonstrated (*9*, *14*, *20*, *21*).

RESULTS

Deletion of the Atg16L WD domain results in spontaneous AD pathology in mice

To determine the importance of the WD domain of Atg16L in central nervous system physiology, we evaluated aged mice lacking the WD domain of Atg16L (Atg16L$^{\Delta WD}$) (*10*). We observed that 2-year-old mice had robust deposition of endogenous murine Aβ in the hippocampus (Fig. 1, A and B) and throughout the cerebral cortex compared to littermate controls (fig. S1, A to C). Upon closer inspection, Aβ pathology was characterized by a combination of extracellular aggregates and intraneuronal deposits (Fig. 1C). Most Aβ was found to be soluble and consisting of both the Aβ_{1-40} and Aβ_{1-42} neurotoxic peptides (Fig. 1D). Although these findings are consistent with what is typically observed in human patients with AD (*22*), aged mice lacking the WD domain of Atg16L did not present with dense-cored Aβ plaques, characteristic of both human disease and those found in mouse models overexpressing mutant forms of human amyloid precursor protein (APP), as there was a lack of increased insoluble Aβ (Fig. 1D). It is plausible that the lack of plaque formation is a result of inherent biochemical differences between endogenous mouse and human APP and the associated Aβ-cleavage products. In particular, mouse Aβ_{1-42} has a reduced propensity for forming β-sheet structures compared to human Aβ_{1-42}, which may explain the absence of Aβ plaques in WD domain–deficient mice where endogenous mouse Aβ peptides are accumulating (*23*).

We also observed pervasive hyperphosphorylation of the microtubule-stabilizing protein Tau in the hippocampus (Fig. 2, A and B) with pronounced accumulation in the CA3 field (Fig. 2C) and throughout the brain as a whole (Fig. 2D and fig. S1D). The proline-directed kinase–dependent phosphorylation of Tau at serine residues 199 and 202 (S199/S202) is highly correlative to Tau phosphorylation observed in human AD (*24*). The S202 phosphorylation is a major contributing phosphorylation event in the development of human neurofibrillary tangles, defined as aggregates of hyperphosphorylated Tau and are a known disease-relevant epitope leading to synaptic and neuronal dysfunction (*25*–*27*). Consistent with observations in human AD brain (*26*, *28*), Tau hyperphosphorylation was not restricted to a singular phosphorylation event. Phosphorylation of Tau at S404 and S416 was likewise substantially elevated in Atg16L WD domain–deficient mice (Fig. 2D). Moreover, the phosphorylation present in the Atg16L$^{\Delta WD}$ mice is on endogenous Tau, driven entirely by the sole genetic manipulation of the Atg16L WD domain. This Tau pathology is therefore fully independent of either ectopic or overexpression of human Tau or mutants of human Tau, models

[1]Department of Immunology, St. Jude Children's Research Hospital, Memphis, TN, USA. [2]Department of Developmental Neurobiology, St. Jude Children's Research Hospital, Memphis, TN, USA. [3]School of Biological Sciences, University of East Anglia, Norwich, Norfolk, UK. [4]Quadram Institute of Bioscience, Norwich, Norfolk, UK. [5]Norwich Medical School, University of East Anglia, Norwich, Norfolk, UK.
*Corresponding author. Email: brad.heckmann@stjude.org (B.L.H.); douglas.green@stjude.org (D.R.G.)

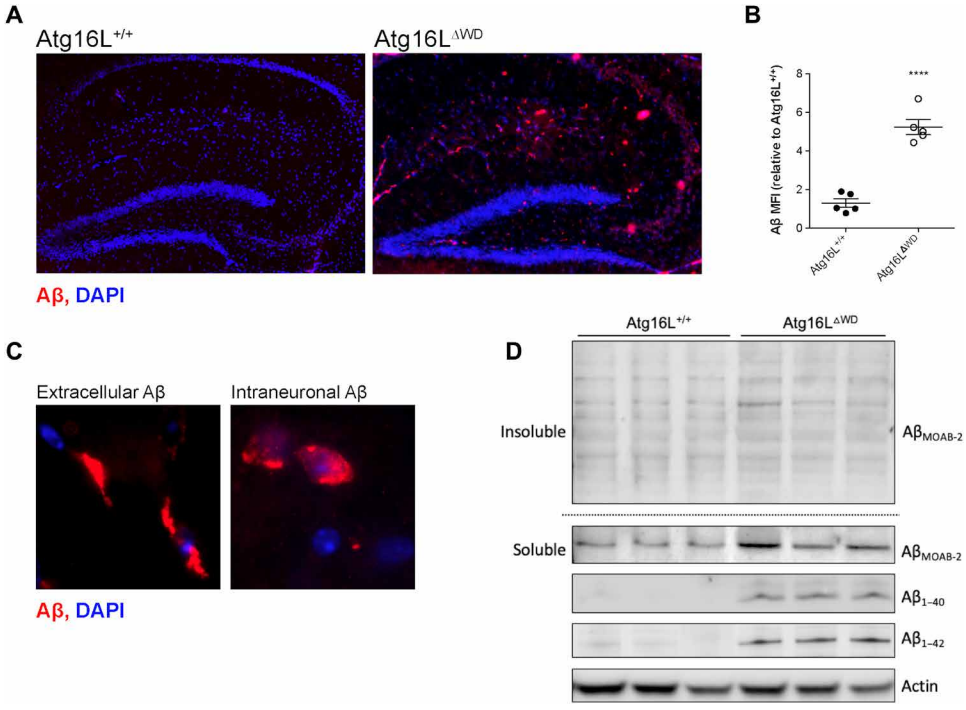

Fig. 1. Aged mice lacking the WD domain of Atg16L have robust Aβ deposition. All mice analyzed at 2 years of age, unless otherwise noted. (**A**) Representative immunofluorescence imaging of hippocampal Aβ. (**B**) Quantification of Aβ mean fluorescent intensity (MFI) in the hippocampus; each point represents an individual mouse. (**C**) High-resolution representative imaging of both extracellular and intraneuronal Aβ deposits in hippocampus. (**D**) Immunoblot analysis of whole-brain lysates for soluble and insoluble Aβ, C99 fragment using the MOAB-2 antibody and specific analysis of Aβ neurotoxic peptides 1 to 40 and 1 to 42. DAPI, 4′,6-diamidino-2-phenylindole. ****$P < 0.0001$.

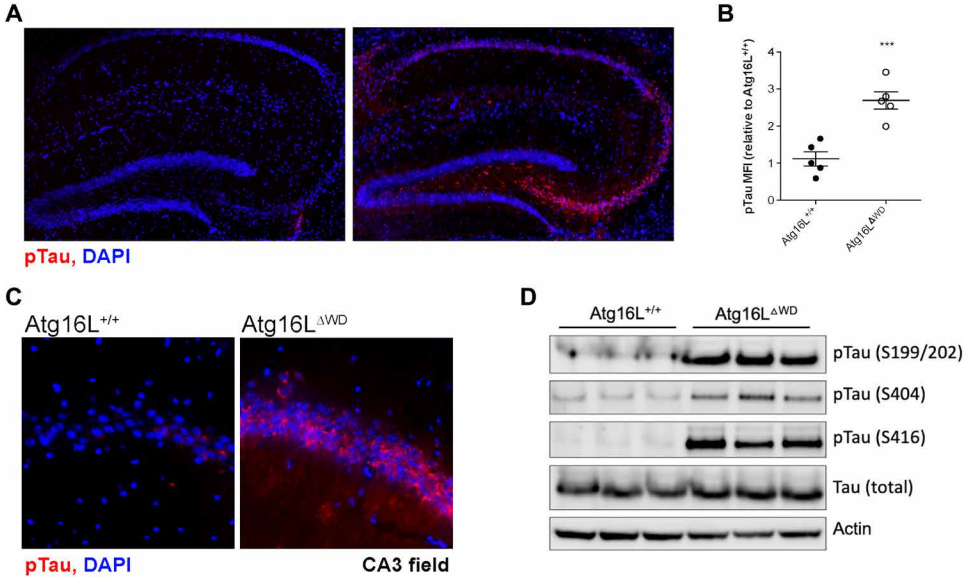

Fig. 2. Aged mice lacking the WD domain of Atg16L have robust Tau hyperphosphorylation. (**A**) Representative imaging of S199/202 Tau phosphorylation in hippocampus. (**B**) Quantification of Tau phosphorylation in the hippocampus; each point represents and individual mouse. (**C**) CA3 field–specific imaging of S199/202 Tau phosphorylation. (**D**) Immunoblot analysis of whole brain for multiple species of phospho-Tau (pTau) compared to total-Tau. Actin was used as a loading control. ***$P < 0.001$.

frequently used to study these and other Tau phosphorylation events and associated physiological consequences.

Since aged Atg16L$^{\Delta WD}$ mice had robust Aβ deposition and Tau hyperphosphorylation, we asked how the loss of the WD domain was contributing to endogenous Aβ accumulation. It has been shown that components of the autophagy machinery are required for the recycling of Aβ receptors in a process known as LC3-associated endocytosis (LANDO) (*14*), and defects in this recycling can lead to

accumulation of Aβ in the transgenic 5xFAD model (*5*, *14*). Therefore, to interrogate a plausible mechanism leading to Aβ deposition, we evaluated LANDO-dependent recycling of the Aβ receptors TREM2 (Triggering Receptor Expressed On Myeloid Cells 2), CD36, and Toll-like receptor 4 (TLR4) (*29*, *30*) and the contribution of the WD domain of Atg16L to this process. We found that recycling of all three receptors was contingent on the WD domain of Atg16L in primary microglia, consistent with a putative role for this domain in the LANDO pathway (Fig. 3, A and B). This impairment in LANDO-dependent recycling led to the decreased secondary uptake of Aβ in primary microglia lacking the WD domain of Atg16L (Fig. 3C). Therefore, failed Aβ clearance through loss of LANDO may contribute to the observed accumulation in vivo, as suggested previously (*14*). It is important to note, however, that the WD domain of Atg16L has roles in other pathways marked by LC3-lipidation at single membranes, including xenophagy and LC3-associated phagocytosis (*9*, *10*, *31*). Therefore, the abrogation of LANDO by deletion of the Atg16L WD domain may not be exclusively responsible for the Aβ deposition observed in the aged Atg16L$^{\Delta WD}$ animals. However, it was evident that the effects observed are likely independent of canonical autophagy, as deletion of the WD domain of Atg16L had no effect on the autophagy markers P62 (Sequestosome-1) and LC3-II in either whole brain or in ex vivo brain cultures treated with an inhibitor of lysosomal acidification (fig. S2, A and B). Together, these data suggest that full-length Atg16L is required for the LANDO-dependent recycling of Aβ receptors in microglia, and loss of the WD domain of Atg16L is sufficient to drive AD pathology of endogenous murine Aβ and Tau in a process independent of canonical autophagy.

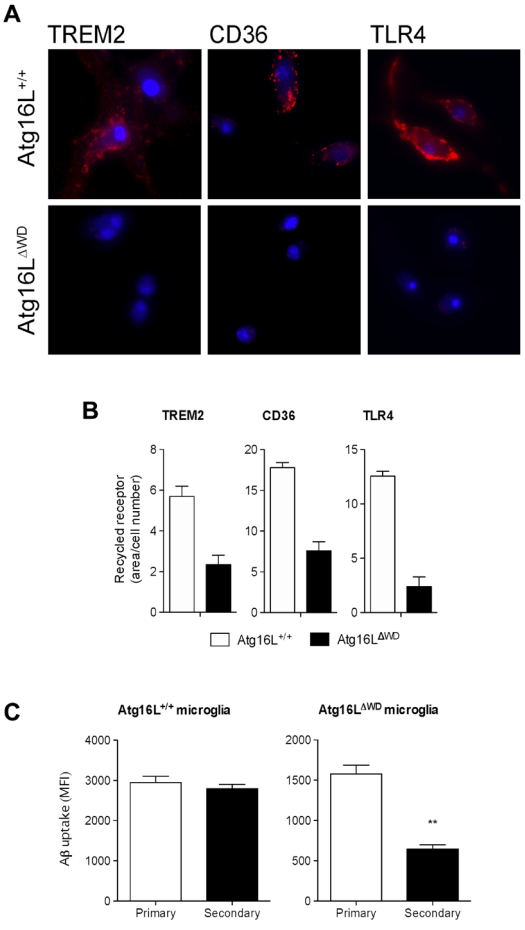

Fig. 3. Atg16L WD domain deletion leads to impaired recycling of Aβ receptors and decreased Aβ uptake. (**A**) Representative image of receptor recycling for TREM2, CD36, and TLR4 in primary microglia of the indicated genotypes. (**B**) Quantification of receptor recycling depicted as fluorescent area/total cell number. $n = 4$ performed in triplicate. (**C**) Secondary Aβ uptake measured in primary microglial cells of the indicated genotype. $n = 3$ performed in triplicate. $^{**}P < 0.01$ and $^{***}P < 0.001$.

Mice lacking the WD domain of Atg16L display robust neuroinflammation

A consequence of Aβ deposition in human disease and murine models of AD is the proinflammatory activation of microglia (*32*). We observed exacerbated activation of microglia in the hippocampi of mice lacking the WD domain of Atg16L compared to wild-type littermates at 2 years of age (Fig. 4, A and B). As observed with Aβ and phospho-Tau, microglial activation was not restricted to the hippocampus and was prevalent throughout the cortex (Fig. 4, C and D). In addition to up-regulation of Iba1 (Ionized calcium binding adaptor molecule 1), microglia in aged Atg16L$^{\Delta WD}$ mice displayed a transition from ramified to ameboid morphology (Fig. 4E), consistent with inflammatory polarization (*33*). The proinflammatory cytokines interleukin-1β (IL-1β), IL-6, and tumor necrosis factor–α (TNFα) are often elevated in brains of patients with AD and are known to be major components in disease progression (*34*). Consistent with this, we found that the aged Atg16L$^{\Delta WD}$ had increased neuroinflammation, as determined by measuring the expression of IL-1β, IL-6, and TNFα in the hippocampus when compared to littermate controls, again paralleling healthy versus AD pathology in humans (Fig. 4F).

Atg16L WD domain deficiency leads to neurodegeneration in aged mice

Since we observed endogenous Aβ deposition, Tau phosphorylation, and neuroinflammation, all of which are risk factors for impaired neuronal function, we profiled the neuronal architecture and function in Atg16L WD domain–deficient mice. Compared to control littermates, 2-year-old Atg16L$^{\Delta WD}$ mice had widespread cleavage of caspase 3, consistent with apoptotic death (Fig. 5, A to C). In agreement with cleavage of caspase 3, 2-year-old Atg16L$^{\Delta WD}$ mice had an increase in terminal deoxynucleotidyl transferase–mediated deoxyuridine triphosphate nick end labeling–positive (TUNEL^{+}) neurons compared to wild-type animals, indicative of apoptosis and suggestive of active neurodegeneration (Fig. 5D). Moreover, 2-year-old Atg16L$^{\Delta WD}$ mice had a robust reduction in total neurons within the hippocampus, quantified using the neuronal nuclei marker NeuN (fig. S3A). These data suggest that aged mice lacking the WD domain of Atg16L have an increased susceptibility for neuronal death and Aβ-associated neuroinflammation.

We next evaluated the physiological function of neurons within the hippocampus. We hypothesized that apoptotic processes would affect synaptic function. Basal synaptic transmission at excitatory synapses between hippocampal CA3 and CA1 pyramidal neurons (CA3-CA1 synapses) was not affected in 2-year-old mice lacking the WD domain of Atg16L when compared to control littermates (fig. S3B). However, 2-year-old Atg16L$^{\Delta WD}$ mice had a substantial reduction in long-term potentiation (LTP) at CA3-CA1 synapses (Fig. 5E). While the deposition of neurotoxic Aβ peptides has been linked to impairments in synaptic plasticity in humans (*35*, *36*), recent evidence suggests that soluble, nonfibrillary, or plaque-bound Aβ species are

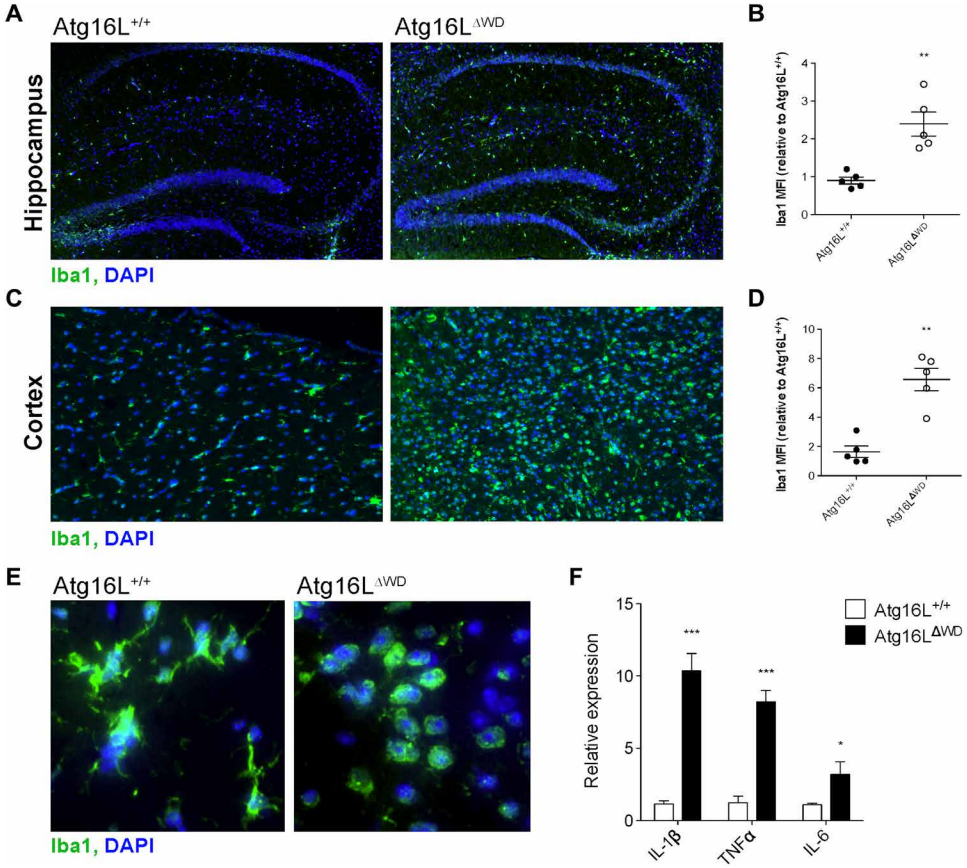

Fig. 4. Atg16L WD domain deletion results in reactive microgliosis and neuroinflammation. All mice were analyzed at 2 years of age, unless otherwise noted. (**A**) Representative immunofluorescence imaging of hippocampal microglial activation, as measured by Iba1. (**B**) Quantification of Iba1 MFI in the hippocampus; each point represents an individual mouse. (**C**) Representative imaging of microglial activation by Iba1 in the cerebral cortex. (**D**) Quantification of Iba1 MFI in the cerebral cortex; each point represents an individual mouse. (**E**) Morphological analysis of microglia marked by Iba1. (**F**) Quantitative PCR (qPCR) analysis of inflammatory cytokine expression from isolated hippocampi; $n = 5$ performed in triplicate. $^{***}P < 0.001$, $^{**}P < 0.01$, and $^{*}P < 0.05$.

more detrimental to synaptic function, as measured by impaired LTP and characterized by increases in neuroinflammation (*37*–*39*). Our findings herein regarding Aβ deposition in nonplaque-like structures and the effects observed on LTP in the aged mice are notably similar to what has been shown in human AD brain samples (*40*).

As a consequence of reduced LTP, Atg16L$^{\Delta WD}$ mice presented with severe behavioral and memory deficiencies. Performances in the sucrose preference test (SPT), spontaneous alternation (Y-maze), and novel object recognition (NOR) were all drastically impaired in 2-year-old mice lacking the WD domain of Atg16L compared to littermate controls (Fig. 5, F to I). No measurable differences in fluid intake or total number of arm entries for Atg16L$^{\Delta WD}$ mice compared to wild-type for the SPT and Y-maze, respectively, were observed (fig. S3, C and D). Atg16L$^{\Delta WD}$ mice displayed a trend toward increased total exploration time during the NOR (fig. S3E). Although this effect was not significant, it is consistent with previous reports in both mice and humans with AD, where the exploration time is typically increased to offset the inability to discern either the object (mice) or the locale (human).

The aged Atg16L WD domain–deficient mice were produced on a mixed (C57BL6/J,129) background and were not fully inbred (*10*). Therefore, we performed a single-nucleotide polymorphism (SNP) background analysis and compared percentage of background strain to disease markers, including spontaneous alternation (behavioral) and Aβ burden (pathological). No discernable influence of the prevailing background strain was observed for either marker of disease (fig. S4A). As a whole, these data demonstrate that the loss of the WD domain of Atg16L and the associated upstream pathology leads to neuroinflammation, neurodegeneration, dysfunction in synaptic plasticity, and severe behavioral impairment consistent with highly progressive disease.

Inhibition of neuroinflammation alleviates AD pathology in Atg16L$^{\Delta WD}$ mice

Our results indicated that deletion of the WD domain of Atg16L leads to the age-associated development of an endogenous, spontaneous AD pathology in mice. We next asked whether the observed pathology and memory impairment could be reversed once established and to what extent of the behavioral pathology was a consequence of neurodegeneration compared to neuroinflammation. Inflammasome inhibition has been proposed as a putative therapeutic approach that reduces neuroinflammation and Tau phosphorylation (*41*–*45*). Therefore, we treated Atg16L WD domain–deficient mice with established disease (starting at 20 months of age) and behavioral impairment, as measured by both impaired spontaneous alternation and NOR (fig. S5, A and B) with the brain-penetrant inflammasome

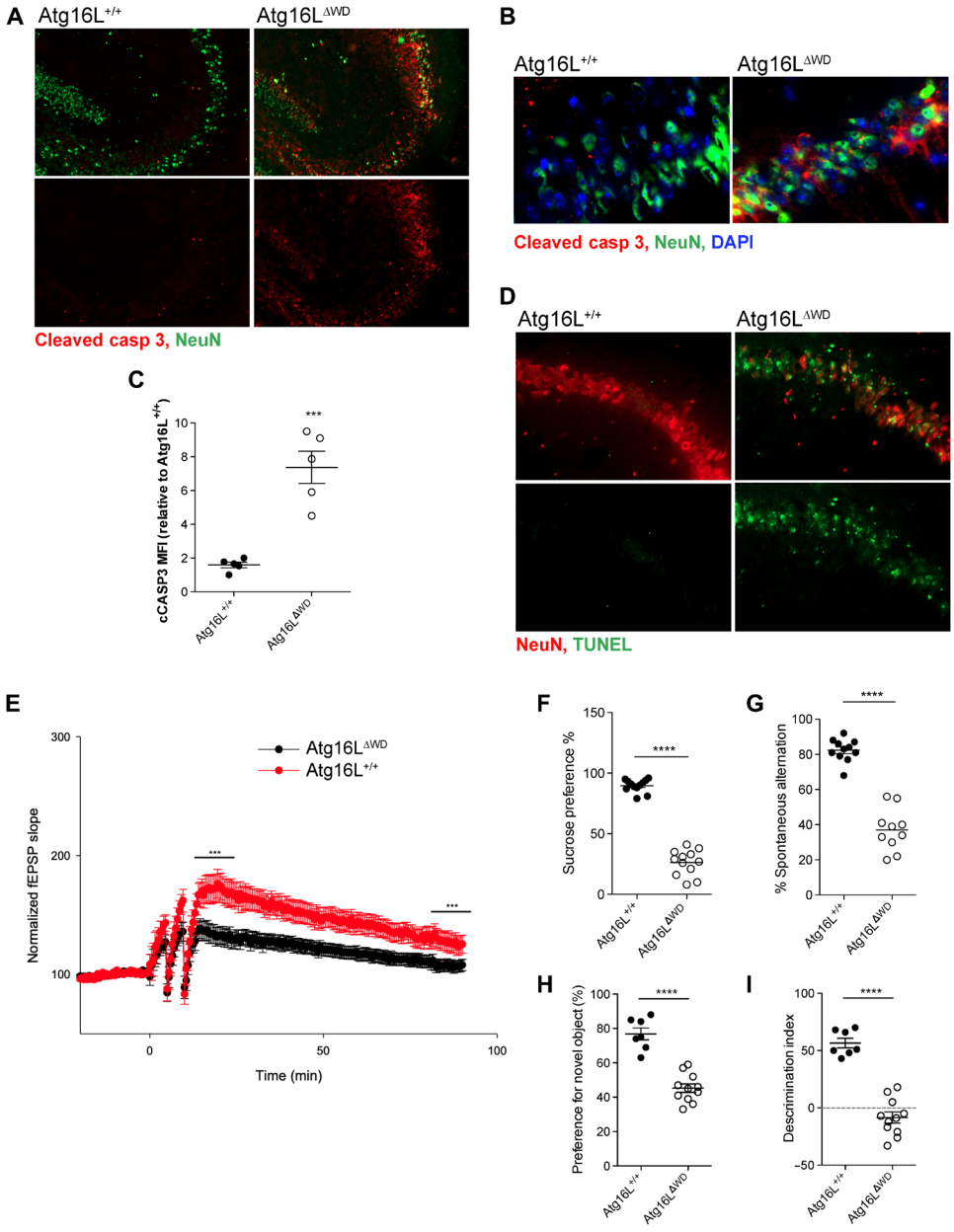

Fig. 5. Mice lacking the WD domain of Atg16L have active neurodegeneration, impaired synaptic plasticity, and memory impairment. All mice were analyzed at 2 years, of age unless otherwise noted. (**A**) Representative immunofluorescence imaging of neuronal cleaved caspase 3 staining. (**B**) High-resolution imaging of hippocampal cleaved caspase 3 staining of neurons. (**C**) Quantification of cleaved caspase 3 MFIs in the hippocampus; each point represents an individual mouse. (**D**) Representative immunofluorescence of hippocampal TUNEL staining. (**E**) Hippocampal LTP is reduced in Atg16L WD domain–deficient mice. Normalized CA3-CA1 field excitatory postsynaptic potentials (fEPSPs) as a function of time before and after induction of LTP. (**F**) Sucrose preference as measured as a percentage compared to standard water. (**G**) Spontaneous alternation percentage, as measured by Y-maze analysis. Novel object (**H**) preference and (**I**) discrimination index, as measured by NOR analysis. ***$P < 0.001$ and ****$P < 0.0001$.

inhibitor MCC950 (*46*–*50*). Following 8 weeks of treatment, we observed reduced levels of microglial activation in mice treated with MCC950 compared to control (Fig. 6A and fig. S6A). Moreover, there was a reduction in both cleaved IL-1b and cleaved caspase 1 in the brains of mice treated with MCC950, indicative of effective inflammasome inhibition (Fig. 6B). However, no differences in Aβ deposition between control and treated animals were observed (fig. S6B). Inhibition of neuroinflammation resulted in a marked reduction in both Tau phosphorylation (Fig. 6C and fig. S6C) and neurodegeneration, as measured by TUNEL staining (Fig. 6D).

Consequently, mice treated with MCC950 had a restoration in their behavioral and memory capacity, approaching that of wild-type littermates in both the Y-maze (Fig. 6E) and NOR (Fig. 6F) assays, with control-treated mice continuing to exhibit behavioral decline when compared to treatment onset (fig. S5, A and B). No differences in arm entries or the exploration time were observed

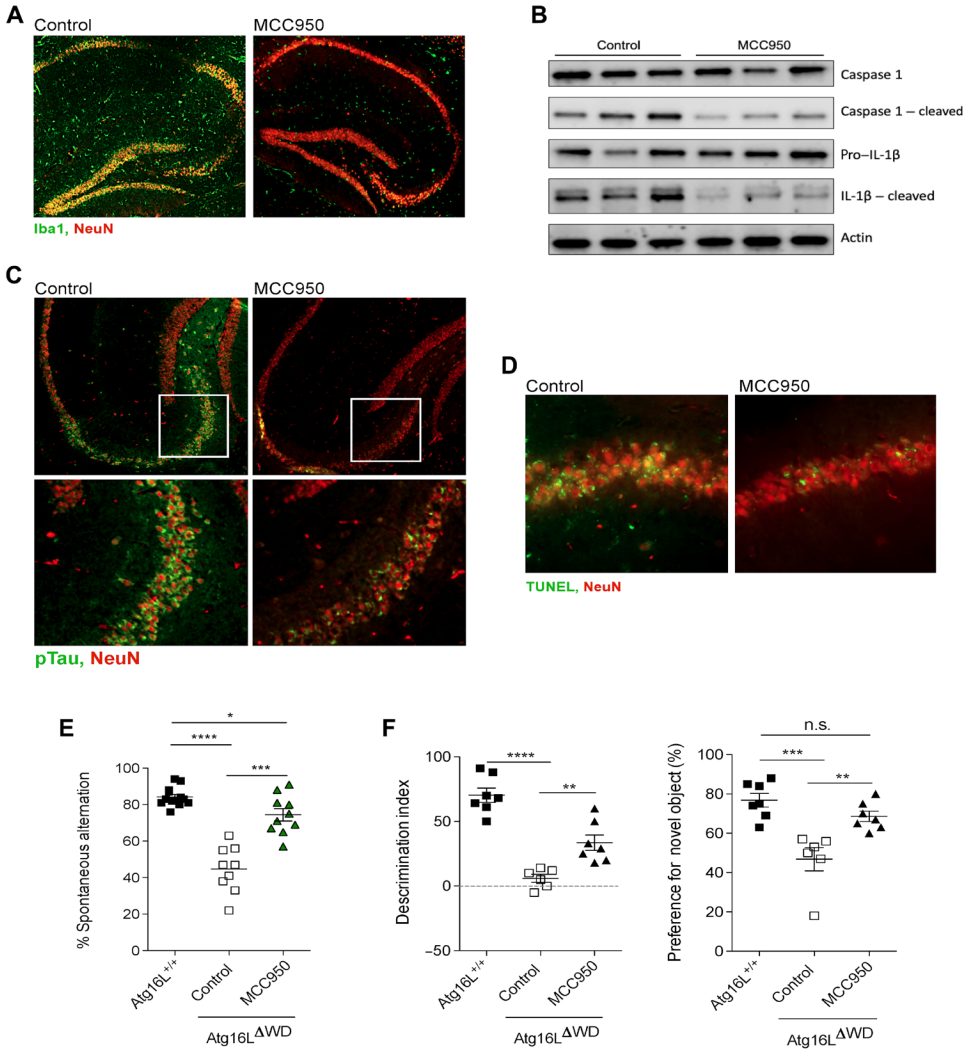

Fig. 6. Therapeutic response following inhibition of neuroinflammation in Atg16L WD-deficient mice with established AD pathology. Mice were treated as control or with MCC950 for 8 weeks. (**A**) Representative imaging of microglial activation by the Iba1 expression in the hippocampus. (**B**) Immunoblot analysis of inflammasome inhibition following MCC950 treatment. (**C**) Representative imaging of S199/202 Tau phosphorylation in CA3 field of the hippocampus. (**D**) Representative imaging of hippocampal cell death by TUNEL. (**E**) Spontaneous alternation percentage, as measured by Y-maze analysis. (**F**) Novel object preference and discrimination index, as measured by NOR analysis. *$P < 0.05$, **$P < 0.01$, ***$P < 0.001$, and ****$P < 0.0001$. n.s., not significant.

between the control and treated groups (fig. S6, D and E). Together, these results suggest that neuroinflammation is upstream of Tau phosphorylation and progressive neurodegeneration in AD pathology and contributes to behavioral deficits beyond those caused by neuronal loss.

Regulators of LANDO, including Atg16L, are down-regulated in human AD

Since we observed a strong AD phenotype resulting from the abrogation of Atg16L function and robust neuroinflammation in mice deficient in the WD domain of Atg16L, we asked whether there were correlations between Atg16L and disease in human brain. Mixed sex and age cohorts of normal (healthy) versus AD human brain samples were analyzed (Fig. 7A). All AD samples were established as diseased before analysis and were confirmed for Aβ burden (Fig. 7B). We first evaluated the expression of transcription factors involved in the regulation of genes associated with both canonical and non-canonical autophagic functions (*51*, *52*). We observed marked decreases in master regulators, including transcription factor EB (TFEB) and Eukaryotic Translation Initiation Factor 5A (EIF5α), and decreased transcription of components of the machinery that regulates LANDO, including Rubicon (Fig. 7C). Furthermore, we observed likewise decreases in the protein expression of Atg16L, Rubicon, and Atg5 and, to a lesser extent, FAK family kinase-interacting protein of 200 kDa (FIP200) in the diseased patient samples compared to non-AD, normal samples (Fig. 7, D and E). These results are consistent with previous findings regarding decreased expression of autophagy genes with age and further in AD (*53*–*55*); however, we directly found decreases in two key regulators of LANDO (Atg16L and Rubicon), which have, to date, not been described. Although these data are not sufficient to directly link defects in the LANDO machinery with AD establishment in humans, they do illustrate a relationship between the expression of the LANDO machinery and AD that is correlative to disease pathology in the spontaneous age-associated AD observed in the Atg16L WD-deficient mouse.

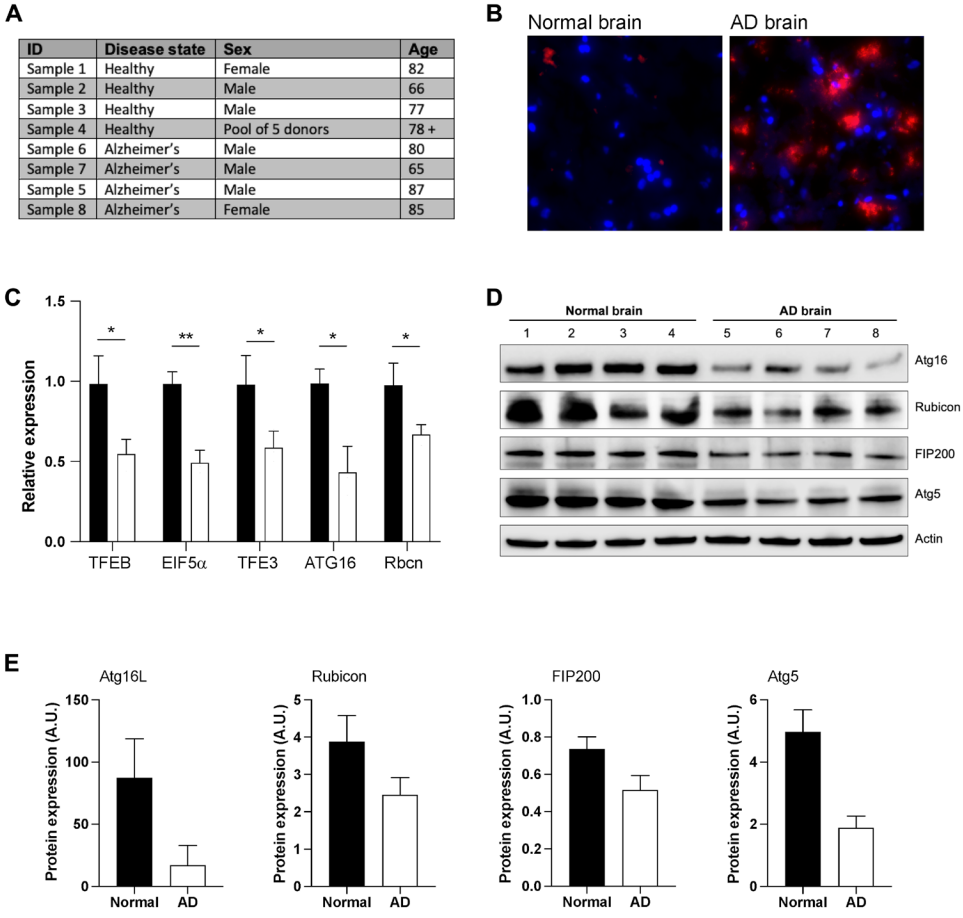

Fig. 7. Down-regulation of LANDO machinery in human AD. (**A**) Identification and information on normal and patients with AD–derived samples used. (**B**) Representative immunofluorescence imaging showing Aβ deposition in normal versus AD samples to confirm disease state. (**C**) qPCR analysis of transcriptional regulators and components of the LANDO machinery from whole-brain RNA. (**D**) Immunoblot analysis of components comprising the LANDO or autophagy machinery in whole-brain lysates. (**E**) Quantification of protein expression. *$P < 0.05$ and **$P < 0.01$. Rbcn, Rubicon; A.U., arbitrary units.

DISCUSSION

Previously, we demonstrated that ablation of components of LANDO in microglia markedly exacerbate AD pathology in a transgenic murine model (5xFAD) (*20*). Our findings reported herein indicate that deletion of a single domain of the autophagy protein Atg16L, required for LANDO, is sufficient for driving spontaneous, age-associated AD pathology in mice. This represents a novel endogenous establishment of AD in mice that recapitulates the primary markers of human disease in the absence of overexpression of human disease drivers including mutant forms of APP, presenilin 1, or Tau. Although we do not have direct evidence linking deficiencies in LANDO or other noncanonical functions of the autophagy machinery to AD in humans, we observed a down-regulation in the expression of components of the LANDO machinery in human patients with AD. It is tempting to speculate that chronic or sustained suppressions in the expression of this machinery, as suggested previously (*14*) and consequential impairment in LANDO, are contributing factors to the establishment and progression of AD in humans, likely through increased neuroinflammatory processes.

We observed that deficiency in the WD domain of Atg16L led to Aβ deposition that was highly characterized by soluble Aβ peptides 1 to 40 and 1 to 42, both of which are highly neurotoxic and neuroinflammatory (*56*–*58*) and have been theorized as primary drivers of AD, more so than fibrillary or plaque-associated Aβ (*59*, *60*). Central to this idea is the induction of neuroinflammation by soluble Aβ peptides (*14*, *61*), which is observed in the WD domain–deficient mice. We further found that established disease in this model can be reversed through inhibition of neuroinflammation. Decreased neuroinflammation led to reduced Tau phosphorylation and reductions in active neuronal cell death, leading to improved cognitive function, suggesting that sustained neuroinflammation directly affects the ability of neurons to signal, in addition to functioning as a primary driver of neuronal death. Some previous studies evaluating the efficacy of targeting neuroinflammation in AD have observed decreases in Aβ burden following inflammasome inhibition (*42*, *44*, *47*). However, we failed to see any reduction in Aβ deposition following MCC950 treatment. The sustained Aβ deposition we observe is likely a result of the inability to efficiently clear Aβ as a consequence of impaired LANDO at the genetic level, which we have reported previously (*14*).

It is clear that exacerbated and sustained neuroinflammation is a key component in the establishment and progression of AD and that noncanonical functions of the autophagy machinery in pathways such as LANDO, which are correlative to AD in humans, are

critical regulators of inflammatory activation in response to Aβ. The mechanism by which LANDO is able to link Aβ recognition with inflammatory regulation remains elusive; however, it is plausible that the reduced recycling of Aβ receptors leads to sustained intracellular signaling following receptor activation. Likewise, it is plausible that a direct interaction between the $LC3^+$ endosome containing Aβ and downstream inflammatory complexes such as the NOD-, LRR- and pyrin domain-containing protein 3 (NLRP3) inflammasome exists; however, currently, this is speculative.

Cumulatively, we found that singular alterations in components of the LANDO pathway are sufficient to drive pervasive, spontaneous AD. Furthermore, we suggest that neuroinflammation is centric to AD establishment and progression upstream of neurodegeneration and can be suppressed by LANDO. Last, we show that targeting neuroinflammation is a viable therapeutic approach to prevent neurodegeneration and restore cognitive function.

MATERIALS AND METHODS

Reagents, antibodies, and qPCR oligos

The following primary antibodies were used for immunofluorescence staining, immunoblot, and/or receptor recycling assays: anti-Aβ MOAB-2 (Novus Biologicals, NBP2-13075), anti-$Aβ_{1–42}$ specific (EMD Millipore, AB5078P), anti-$Aβ_{1–40}$ specific (AbBiotec, 251360), anti-S199/202 Tau (Thermo Fisher Scientific, 44-768G), anti-S404 Tau (Cell Signaling Technology , 35834), anti-S416 Tau (Cell Signaling, 15013), anti-Tau (Cell Signaling, 46687), anti-Iba1 (Novus, NB100-1028), anti-NeuN (Abcam, ab177487), anti–cleaved caspase 3 (Cell Signaling, 9664), anti–β-actin horseradish peroxidase (HRP; Thermo, MA1-91399), anti-LC3 (Cell Signaling, 2775), anti-p62 (Sigma, P0067), anti-TREM2 (R&D Systems, MAB17291), anti-CD36 (Abcam, ab23680), anti-TLR4 (Abcam, ab22048), anti–IL-1β (Cell Signaling, 12703), anti–cleaved IL-1β (Cell Signaling, 83186), anti–caspase 1 (Cell Signaling, 3866), anti–cleaved caspase 1 (Cell Signaling, 4199), anti-Rubicon (Cell Signaling, 8465), anti-FIP200 (Cell Signaling, 12436), and anti-Atg5 (Cell Signaling, 12994). TUNEL staining was achieved using the Click-iT TUNEL Alexa Fluor 488 (AF488) Imaging Assay kit (Invitrogen) according to the manufacturer's instructions on brain sections prepared and imaged, as described below. $Aβ_{1–42}$ labeled with either AF488 or TAMRA was purchased from AnaSpec and prepared for the Aβ uptake assay, as described previously (*14*).

The following oligos (IDT; Integrated DNA Technologies) were used for reverse transcription polymerase chain reaction (RT-PCR; represented as 5′-3′ for each primer): actin, ATGGAGGGGAATACAGCCC (forward) and TTCTTTGCAGCTCCTTCGTT (reverse); Iba1, CAGACTGCCAGCCTAAGACA (forward) and AGGAATTGCTTGTTGATCCC (reverse); TNFα, CCTGTAGCCCACGTCGTAGC and AGCAATGACTCCAAAGTAGACC (reverse); IL-1β, CACAGCAGCACATCAACAAG (forward) and GTGCTCATGTCCTCATCCTG (reverse); IL-6, GAGGATACCACTCCCAACAGACC (forward) and AAGTGCATCATCGTTGTTCATACA (reverse); TFEB, CCTGGAGATGACCAACAAGCAG (forward) and TAGGCAGCTCCTGCTTCACCAC (reverse); EIF5α, GAGCAGAAGTACGACTGTGGAG (forward) and CAGGTTCAGAGGATCACTGCTG (reverse); TFE3, GATCATCAGCCTGGAGTCCAGT (forward) and AGCAGATTCCCTGACACAGGCA (reverse); Atg16L1, CTACGGAAGAGAACCAGGAGCT (forward) and CTGGTAGAGGTTCCTTTGCTGC (reverse); and Rubicon, CCTGCTCGGGGATAGACAGTA (forward) and CTGGCAAACATGGACGCATC (reverse).

Mice

Deletion of the WD domain of Atg16L ($Atg16L^{ΔWD}$) was achieved, as previously described (*10*). In brief, two stop codons were immediately inserted into exon 6 of murine Atg16L1 after glutamate E230 to preserve binding sites for WIPI2 (WD Repeat Domain, Phosphoinositide Interacting 2) (required for canonical autophagy) but prevent translation of the linker and WD domain. Mice were produced and maintained on a mixed 129, C57BL/6 background.

Unless otherwise noted, all experiments were performed on mixed-sex cohorts at 2 years of age. Mice treated with MCC950 or vehicle control were mixed-sex cohorts, 20 months of age at time of treatment onset, and were treated for 8 weeks, as described below. Mice were produced and aged at the University of East Anglia in accordance with the U.K. Home Office guidelines and under the U.K. Animals (Scientific Procedures) Act 1986. All mice were housed in pathogen-free facilities, in a 12-hour light/dark cycle in ventilated cages, with chow and water supply ad libitum before, during, and following transfer from the University of East Anglia to St. Jude Children's Research Hospital. All mice were allowed to acclimate for a period of at least 6 weeks before analysis or experimental usage. The St. Jude Institutional Animal Care and Use Committee approved all procedures in accordance with the *Guide for the Care and Use of Animals*.

The genetic backgrounds of mice used were assessed at the DartMouse Speed Congenic Core Facility at the Geisel School of Medicine at Dartmouth. DartMouse uses the Illumina Inc. (San Diego, CA) Infinium genotyping assay to interrogate a custom panel of 5307 SNPs spread throughout the genome. The raw SNP data were analyzed using DartMouse's SNaP-Map and Map-Synth software, allowing the determination for each mouse of the genetic background at each SNP location. Background strain percentage was subsequently compared against markers of disease pathology to evaluate any influence stemming from variations in background (see fig. S3A).

Human samples

Commercial protein and RNA lysates from whole brain of either normal or AD donors were purchased from Biochain and Novus Biologicals. Lysates used for immunoblot analysis were prepared according to the manufacturer's instructions. Total RNA lysates were processed for complementary DNA, as described below. Donor information was provided by the supplier and is included herein.

MCC950 inflammasome inhibition in vivo

Mice with established disease (described above) were treated for 8 weeks with either a vehicle (control) or MCC950 (Invivogen), as reported previously (*46*). In brief, MCC950 was suspended in 100% dimethyl sulfoxide (DMSO) and titrated to a working dose using sterile water. The final concentration of DMSO in the injection was <1%. Matching solution without MCC950 was used as the vehicle (control). Mice were injected every 3 days for 8 weeks at a dose of 10 mg/kg via intraperitoneal injection.

Primary microglial isolation and culture

Primary microglia were isolated from $Atg16L^{ΔWD}$ or littermate $Atg16L^{+/+}$ control animals, as described previously (*50*). Isolated cells

were subsequently cultured and maintained in complete Dulbecco's modified Eagle's medium (DMEM) [10% fetal bovine serum, 200 mM L-glutamine, and penicillin-streptomycin (100 U/ml)] at 37°C with 5% CO_2.

Microscopy and image analysis

Cells were cultured in four-well chamber slides (Ibidi) and were fixed and stained, as indicated. In brief, cells were fixed with 4% paraformaldehyde (PFA) for 10 min. Followed by permeabilization using 0.1% Triton X-100 for 5 min. Cells were blocked in 0.5% bovine serum albumin (BSA) in phosphate-buffered saline (PBS) for 30 min before staining with primary antibodies overnight at 4°C. Cells were then washed three times in PBS and then stained with the indicated fluorescent secondary antibodies for 30 min. Cells were subsequently washed three times with PBS and postfixed in 1% PFA for 10 min before imaging. For all live-cell–based imaging, cells were immediately transferred to an environment-controlled, live-cell imaging chamber (Ibidi).

For preparation of brain tissue, see the "Preparation of brain samples" section below. Slides were subjected to antigen retrieval using 1% sodium citrate boiling for 20 min, followed by three times PBS washing. Slides were blocked in 0.5% BSA in PBS. Antibody staining was carried out, as described above. Following final washing, slides were mounted using the ProLong Diamond Anti-Fade mounting medium with 4′,6-diamidino-2-phenylindole.

All imaging was performed on either an Eclipse Ti-E TIRF/N-Storm/epifluorescence microscope (Nikon) or a Marianis spinning disk confocal microscope [Intelligent Imaging Innovations (3i)] equipped with an electron-multiplying charge-coupled device camera. Image analysis including all quantification was performed using either Nikon NIS-Elements Advanced Research Imaging software or Slidebook 6 (3i).

Image analysis for relative Aβ, Iba1, and phospho-tau staining was achieved by quantifying the mean fluorescent intensity (MFI) of either Iba1 or phospho-tau signal using NIS elements. Analysis and quantification of microglial morphology were achieved using Slidebook 6 software. Morphological state was determined by measuring cell diameter following three-dimensional reconstruction and confirmed by manual counting/analysis of microglia shape per defined field across multiple areas of each slide.

Preparation of brain samples

Mice were anesthetized with isoflurane and perfused with either ice-cold PBS containing heparin (1 U/ml). Right brain hemispheres were fixed in 4% PFA overnight at 4°C, rinsed in PBS, and incubated overnight at 4°C in 30% sucrose before freezing in a 2:1 mixture of 30% sucrose and optimal cutting temperature compound. Serial 20-μm coronal sections were cut on a cryo-sliding microtome. Cortices and hippocampi of the left brain hemispheres were carefully dissected out and flash frozen for biochemical analysis or processed for RNA isolation.

Cell and tissue lysis and immunoblot

Cells and tissue were lysed in radioimmunoprecipitation assay (RIPA) buffer for 30 min on ice [50 mM tris (pH 7.5), 150 mM NaCl, 1% Triton X-100, 0.5% deoxycholate, 0.1% SDS, protease inhibitor tablet (Roche), 1 mM NaF, 1 mM Na_3VO_4, and 1 mM phenylmethylsulfonyl fluoride]. Samples were boiled and centrifuged. After centrifugation, supernatants were analyzed by SDS–polyacrylamide gel electrophoresis. All blots were imaged using HRP-conjugated secondary antibodies and enhanced chemiluminesence using a LI-COR Odyssey Fx imaging system (LI-COR Biosciences). All immunoblot analyses were performed using LI-COR Image Studio software. Primary antibodies used for immunoblotting analysis are listed in the "Reagents, antibodies, and qPCR oligos" section above.

Autophagy analysis in primary brain slices

Brain slices were isolated and cultured, as described previously (*51*, *52*). Slices were maintained in artificial cerebrospinal fluid (ACSF) and were supplemented with PBS vehicle or 25 nM bafilomycin A1 for 3 hours. Following treatment, slices were washed three times with PBS and subsequently homogenized in RIPA buffer, as described above.

Real-time RT-PCR

Total RNA was isolated from cells or tissue using the RNeasy Kit (Qiagen) according to the manufacturer's instructions. First-strand synthesis was performed using the Moloney murine leukemia virus reverse transcriptase (Invitrogen). Real-time PCR was performed using the SYBR Green PCR Master Mix (Applied Biosystems) in an Applied Biosystems 7900HT thermocycler using the SYBR Green Detection protocol, as outlined by the manufacturer using the following PCR conditions: 50°C for 2 min, 95°C for 10 min, and 40 cycles of 95°C for 15 s and 60°C for 1 min. mRNA was normalized to actin allowing for comparison of mRNA levels. Sequences for mouse target primers are detailed in the "Reagents, antibodies, and qPCR oligos" section above.

Receptor recycling

For receptor recycling, cells were plated on four-well Ibidi tissue culture–coated chamber slides and allowed to reach 50% confluence. Cells were then blocked for 15 min in the presence of 10% normal donkey serum at 37°C. Primary antibodies targeting the indicated receptor (see reagent list) were then added at a dilution of 1:100 in 1% donkey serum in DMEM, and cells were incubated at 37°C for 1 hour. Antibody-containing medium was aspirated, and cells were acid washed with a cold DMEM (pH 2.0). Cells were returned to 10% donkey serum in DMEM for 1 hour. Alexa Fluor 568–labeled secondary antibodies were diluted 1:1000 in 1% donkey-serum in DMEM and added to cells for 1 hour at 37°C to label recycled receptors. Cells were subsequently acid washed, as described above, and then fixed in 4% PFA in PBS for 15 min. Cell-permeable Hoechst dye was added to label nuclei.

Following the above protocol, fluorescent signal from recycled receptors is intracellular and readily determined by fluorescent microscopy, as described above. Quantification of recycling was achieved by calculating the sum of AF568-fluorescent area divided by the total number of cells. Nikon NIS-Elements Advanced Research software was used for all image analyses and quantification. This method is well established and used as previously reported (*5*).

Amyloid uptake

Primary and secondary Aβ uptake was assayed as follows. Primary microglia were treated with 1 μM Alexa Fluor 488–labeled $A\beta_{1-42}$. MFI for AF488 was determined by flow cytometry after 12 hours and considered as the primary uptake. The TAMRA-labeled $A\beta_{1-42}$ (1 μM) was subsequently added to the medium following the primary uptake phase. MFI for TAMRA was assessed by flow cytometry 12 hours following the primary uptake time point. This time point constitutes the secondary uptake.

Electrophysiology

Acute transverse hippocampal slices (400 μm) were prepared, as previously described (*62*). Briefly, mouse brains were quickly removed and placed in cold (4°C) dissecting ACSF containing 125 mM choline-Cl, 2.5 mM KCl, 0.4 mM $CaCl_2$, 6 mM $MgCl_2$, 1.25 mM NaH_2PO_4, 26 mM $NaHCO_3$, and 20 mM glucose (285 to 295 mosm) under 95% O_2 and 5% CO_2. After dissection, slices were incubated for 1 hour in ACSF containing 125 mM NaCl, 2.5 mM KCl, 2 mM $CaCl_2$, 2 mM $MgCl_2$, 1.25 mM NaH_2PO_4, 26 mM $NaHCO_3$, and 10 mM glucose (285 to 295 mosm) under 95% O_2 and 5% CO_2 at room temperature and then transferred into the submerged recording chamber and superfused (2 to 3 ml/min) with warm (30° to 32°C) ACSF. The field recordings were performed by using a setup with eight submerged recording chambers (Campden Instruments). The field excitatory postsynaptic potentials (fEPSPs) were recorded from the CA1 stratum radiatum by using an extracellular glass pipette (3 to 5 megohms) filled with ACSF. Schaffer collateral/commissural fibers in the stratum radiatum were stimulated with a bipolar tungsten electrode placed 200 to 300 μm away from the recording pipette.

Behavior and memory analysis

For SPTs, mice were individually house and allowed to acclimate to the testing room for 48 hours before starting the experiment. A dual-bottle setup was introduced where both bottles contained only standard water. Again, mice were allowed to acclimate to the dual-bottle setup for 3 days. After acclimation, one bottle was replaced with a 2% sucrose solution. Water consumption was monitored daily for 4 days. Bottles were rotated daily to minimize side bias and normalized for leakage. All results are shown as the averaged consumption and preference over the 4-day test period.

For Y-maze spontaneous alternation analysis, mice were housed in the testing room and allowed to acclimate for 48 hours. The Y-maze test consisted of a single 5-min trial per mouse. Spontaneous alternation (%) was defined as consecutive entries in three different arms (A, B, and C) divided by the number of possible alternations (total arm entries − 2). Mice with less than 5 arm entries during the 5-min trial were excluded from the analysis.

NOR was performed in an open-field box (40 cm by 40 cm). Mice were allowed to acclimate to the testing room for 48 hours. For habituation, mice were allowed to explore the open field for 15 min per day for 2 days. Mice were then exposed to two identical objects for 10 min on the day of testing. Two hours later, a novel object was introduced, and mice were allowed to explore for 5 min during the test phase. The time spent exploring each object was quantified manually. Novel object preference (%) and the discrimination index [(time with novel)/(novel + familiar) × 100] were calculated for each mouse.

Statistical analysis

Data were plotted and analyzed with GraphPad Prism 7.0 software. Data are represented as mean ± SEM. Significance was calculated using Student's *t* test, unless otherwise noted. All experiments were designed and are powered to a minimum of 0.8, as calculated using G*Power. Differences were considered statistically significant when the *P* value was less than 0.05.

SUPPLEMENTARY MATERIALS

Supplementary material for this article is available at http://advances.sciencemag.org/cgi/content/full/6/33/eabb9036/DC1

View/request a protocol for this paper from *Bio-protocol*.

REFERENCES AND NOTES

1. J. M. Long, D. M. Holtzman, Alzheimer disease: An update on pathobiology and treatment strategies. *Cell* **179**, 312–339 (2019).
2. F. M. Menzies, A. Fleming, A. Caricasole, C. F. Bento, S. P. Andrews, A. Ashkenazi, J. Füllgrabe, A. Jackson, M. J. Sanchez, C. Karabiyik, F. Licitra, A. L. Ramirez, M. Pavel, C. Puri, M. Renna, T. Ricketts, L. Schlotawa, M. Vicinanza, H. Won, Y. Zhu, J. Skidmore, D. C. Rubinsztein, Autophagy and neurodegeneration: Pathogenic mechanisms and therapeutic opportunities. *Neuron* **93**, 1015–1034 (2017).
3. M. M. Lipinski, B. Zheng, T. Lu, Z. Yan, B. F. Py, A. Ng, R. J. Xavier, C. Li, B. A. Yankner, C. R. Scherzer, J. Yuan, Genome-wide analysis reveals mechanisms modulating autophagy in normal brain aging and in Alzheimer's disease. *Proc. Natl. Acad. Sci. U.S.A.* **107**, 14164–14169 (2010).
4. D. C. Rubinsztein, G. Mariño, G. Kroemer, Autophagy and aging. *Cell* **146**, 682–695 (2011).
5. K. M. Lucin, C. E. O'Brien, G. Bieri, E. Czirr, K. I. Mosher, R. J. Abbey, D. F. Mastroeni, J. Rogers, B. Spencer, E. Masliah, T. Wyss-Coray, Microglial beclin 1 regulates retromer trafficking and phagocytosis and is impaired in Alzheimer's disease. *Neuron* **79**, 873–886 (2013).
6. F. Pickford, E. Masliah, M. Britschgi, K. Lucin, R. Narasimhan, P. A. Jaeger, S. Small, B. Spencer, E. Rockenstein, B. Levine, T. Wyss-Coray, The autophagy-related protein beclin 1 shows reduced expression in early Alzheimer disease and regulates amyloid β accumulation in mice. *J. Clin. Invest.* **118**, 2190–2199 (2008).
7. B. L. Heckmann, E. Boada-Romero, L. D. Cunha, J. Magne, D. R. Green, LC3-associated phagocytosis and inflammation. *J. Mol. Biol.* **429**, 3561–3576 (2017).
8. B. L. Heckmann, D. R. Green, LC3-associated phagocytosis at a glance. *J. Cell Sci.* **132**, jcs231472 (2019).
9. K. Fletcher, R. Ulferts, E. Jacquin, T. Veith, N. Gammoh, J. M. Arasteh, U. Mayer, S. R. Carding, T. Wileman, R. Beale, O. Florey, The WD40 domain of ATG16L1 is required for its non-canonical role in lipidation of LC3 at single membranes. *EMBO J.* **37**, e97840 (2018).
10. S. Rai, M. Arasteh, M. Jefferson, T. Pearson, Y. Wang, W. Zhang, B. Bicsak, D. Divekar, P. P. Powell, R. Naumann, N. Beraza, S. R. Carding, O. Florey, U. Mayer, T. Wileman, The ATG5-binding and coiled coil domains of ATG16L1 maintain autophagy and tissue homeostasis in mice independently of the WD domain required for LC3-associated phagocytosis. *Autophagy* **15**, 599–612 (2019).
11. W. H. Yu, A. M. Cuervo, A. Kumar, C. M. Peterhoff, S. D. Schmidt, J.-H. Lee, P. S. Mohan, M. Mercken, M. R. Farmery, L. O. Tjernberg, Y. Jiang, K. Duff, Y. Uchiyama, J. Näslund, P. M. Mathews, A. M. Cataldo, R. A. Nixon, Macroautophagy—A novel β-amyloid peptide-generating pathway activated in Alzheimer's disease. *J. Cell Biol.* **171**, 87–98 (2005).
12. A. Kulkarni, J. Chen, S. Maday, Neuronal autophagy and intercellular regulation of homeostasis in the brain. *Curr. Opin. Neurobiol.* **51**, 29–36 (2018).
13. R. A. Nixon, Autophagy, amyloidogenesis and Alzheimer disease. *J. Cell Sci.* **120**, 4081–4091 (2007).
14. B. L. Heckmann, B. J. W. Teubner, B. Tummers, E. Boada-Romero, L. Harris, M. Yang, C. S. Guy, S. S. Zakharenko, D. R. Green, LC3-associated endocytosis facilitates β-amyloid clearance and mitigates neurodegeneration in murine Alzheimer's disease. *Cell* **178**, 536–551.e14 (2019).
15. D. Doens, P. L. Fernández, Microglia receptors and their implications in the response to amyloid β for Alzheimer's disease pathogenesis. *J. Neuroinflammation* **11**, 48 (2014).
16. M. Ries, M. Sastre, Mechanisms of Aβ clearance and degradation by glial cells. *Front. Aging Neurosci.* **8**, 160 (2016).
17. Y. Wang, M. Cella, K. Mallinson, J. D. Ulrich, K. L. Young, M. L. Robinette, S. Gilfillan, G. M. Krishnan, S. Sudhakar, B. H. Zinselmeyer, D. M. Holtzman, J. R. Cirrito, M. Colonna, TREM2 lipid sensing sustains the microglial response in an Alzheimer's disease model. *Cell* **160**, 1061–1071 (2015).
18. Y. Zhao, X. Wu, X. Li, L.-L. Jiang, X. Gui, Y. Liu, Y. Sun, B. Zhu, J. C. Piña-Crespo, M. Zhang, N. Zhang, X. Chen, G. Bu, Z. An, T. Y. Huang, H. Xu, TREM2 is a receptor for β-amyloid that mediates microglial function. *Neuron* **97**, 1023–1031.e1027 (2018).
19. T. K. Ulland, W. M. Song, S. C.-C. Huang, J. D. Ulrich, A. Sergushichev, W. L. Beatty, A. A. Loboda, Y. Zhou, N. J. Cairns, A. Kambal, E. Loginicheva, S. Gilfillan, M. Cella, H. W. Virgin, E. R. Unanue, Y. Wang, M. N. Artyomov, D. M. Holtzman, M. Colonna, TREM2 maintains microglial metabolic fitness in Alzheimer's disease. *Cell* **170**, 649–663.e13 (2017).
20. J. Martinez, R. K. S. Malireddi, Q. Lu, L. D. Cunha, S. Pelletier, S. Gingras, R. Orchard, J.-L. Guan, H. Tan, J. Peng, T.-D. Kanneganti, H. W. Virgin, D. R. Green, Molecular characterization of LC3-associated phagocytosis reveals distinct roles for Rubicon, NOX2 and autophagy proteins. *Nat. Cell Biol.* **17**, 893–906 (2015).
21. J.-Y. Kim, H. Zhao, J. Martinez, T. A. Doggett, A. V. Kolesnikov, P. H. Tang, Z. Ablonczy, C.-C. Chan, Z. Zhou, D. R. Green, T. A. Ferguson, Noncanonical autophagy promotes the visual cycle. *Cell* **154**, 365–376 (2013).

22. S. Oddo, A. Caccamo, I. F. Smith, K. N. Green, F. M. LaFerla, A dynamic relationship between intracellular and extracellular pools of Aβ. *Am. J. Pathol.* **168**, 184–194 (2006).
23. X. Lv, W. Li, Y. Luo, D. Wang, C. Zhu, Z.-X. Huang, X. Tan, Exploring the differences between mouse mAβ_{1-42} and human hAβ_{1-42} for Alzheimer's disease related properties and neuronal cytotoxicity. *Chem. Commun. (Camb.)* **49**, 5865–5867 (2013).
24. H. Y. Wu, P.-C. Kuo, Y.-T. Wang, H.-T. Lin, A. D. Roe, B. Y. Wang, C.-L. Han, B. T. Hyman, Y.-J. Chen, H.-C. Tai, β-Amyloid induces pathology-related patterns of tau hyperphosphorylation at synaptic terminals. *J. Neuropathol. Exp. Neurol.* **77**, 814–826 (2018).
25. J. P. Brion, Neurofibrillary tangles and Alzheimer's disease. *Eur. Neurol.* **40**, 130–140 (1998).
26. J. Neddens, M. Temmel, S. Flunkert, B. Kerschbaumer, C. Hoeller, T. Loeffler, V. Niederkofler, G. Daum, J. Attems, B. Hutter-Paier, Phosphorylation of different tau sites during progression of Alzheimer's disease. *Acta Neuropathol. Commun.* **6**, 52 (2018).
27. I. Alafuzoff, T. Arzberger, S. Al-Sarraj, I. Bodi, N. Bogdanovic, H. Braak, O. Bugiani, K. Del-Tredici, I. Ferrer, E. Gelpi, G. Giaccone, M. B. Graeber, P. Ince, W. Kamphorst, A. King, P. Korkolopoulou, G. G. Kovács, S. Larionov, D. Meyronet, C. Monoranu, P. Parchi, E. Patsouris, W. Roggendorf, D. Seilhean, F. Tagliavini, C. Stadelmann, N. Streichenberger, D. R. Thal, S. B. Wharton, H. Kretzschmar, Staging of neurofibrillary pathology in Alzheimer's disease: A study of the BrainNet Europe Consortium. *Brain Pathol.* **18**, 484–496 (2008).
28. Y. Zhou, J. Shi, D. Chu, W. Hu, Z. Guan, C.-X. Gong, K. Iqbal, F. Liu, Relevance of phosphorylation and truncation of tau to the etiopathogenesis of Alzheimer's disease. *Front. Aging Neurosci.* **10**, 27 (2018).
29. E. G. Reed-Geaghan, J. C. Savage, A. G. Hise, G. E. Landreth, CD14 and toll-like receptors 2 and 4 are required for fibrillar Aβ-stimulated microglial activation. *J. Neurosci.* **29**, 11982–11992 (2009).
30. M. Song, J. Jin, J.-E. Lim, J. Kou, A. Pattanayak, J. A. Rehman, H.-D. Kim, K. Tahara, R. Lalonde, K.-i. Fukuchi, TLR4 mutation reduces microglial activation, increases Aβ deposits and exacerbates cognitive deficits in a mouse model of Alzheimer's disease. *J. Neuroinflammation* **8**, 92 (2011).
31. Y. Xu, P. Zhou, S. Cheng, Q. Lu, K. Nowak, A.-K. Hopp, L. Li, X. Shi, Z. Zhou, W. Gao, D. Li, H. He, X. Liu, J. Ding, M. O. Hottiger, F. Shao, A bacterial effector reveals the V-ATPase-ATG16L1 axis that initiates xenophagy. *Cell* **178**, 552–566.e20 (2019).
32. Z. Cai, M. D. Hussain, L.-J. Yan, Microglia, neuroinflammation, and beta-amyloid protein in Alzheimer's disease. *Int. J. Neurosci.* **124**, 307–321 (2014).
33. Y. S. Kim, T. H. Joh, Microglia, major player in the brain inflammation: Their roles in the pathogenesis of Parkinson's disease. *Exp. Mol. Med.* **38**, 333–347 (2006).
34. F. Brosseron, M. Krauthausen, M. Kummer, M. T. Heneka, Body fluid cytokine levels in mild cognitive impairment and Alzheimer's disease: A comparative overview. *Mol. Neurobiol.* **50**, 534–544 (2014).
35. M. S. Parihar, G. J. Brewer, Amyloid-β as a modulator of synaptic plasticity. *J. Alzheimers Dis.* **22**, 741–763 (2010).
36. D. J. Selkoe, J. Hardy, The amyloid hypothesis of Alzheimer's disease at 25 years. *EMBO Mol. Med.* **8**, 595–608 (2016).
37. D. Park, S. Chang, Soluble Aβ_{1-42} increases the heterogeneity in synaptic vesicle pool size among synapses by suppressing intersynaptic vesicle sharing. *Mol. Brain* **11**, 10 (2018).
38. C. A. McLean, R. A. Cherny, F. W. Fraser, S. J. Fuller, M. J. Smith, K. Beyreuther, A. I. Bush, C. L. Masters, Soluble pool of Aβ amyloid as a determinant of severity of neurodegeneration in Alzheimer's disease. *Ann. Neurol.* **46**, 860–866 (1999).
39. C. Haass, D. J. Selkoe, Soluble protein oligomers in neurodegeneration: Lessons from the Alzheimer's amyloid β-peptide. *Nat. Rev. Mol. Cell Biol.* **8**, 101–112 (2007).
40. S. Li, M. Jin, L. Liu, Y. Dang, B. L. Ostaszewski, D. J. Selkoe, Decoding the synaptic dysfunction of bioactive human AD brain soluble Aβ to inspire novel therapeutic avenues for Alzheimer's disease. *Acta Neuropathol. Commun.* **6**, 121 (2018).
41. T. Saco, P. T. Parthasarathy, Y. Cho, R. F. Lockey, N. Kolliputi, Inflammasome: A new trigger of Alzheimer's disease. *Front. Aging Neurosci.* **6**, 80 (2014).
42. C. Ising, C. Venegas, S. Zhang, H. Scheiblich, S. V. Schmidt, A. Vieira-Saecker, S. Schwartz, S. Albasset, R. M. McManus, D. Tejera, A. Griep, F. Santarelli, F. Brosseron, S. Opitz, J. Stunden, M. Merten, R. Kayed, D. T. Golenbock, D. Blum, E. Latz, L. Buée, M. T. Heneka, NLRP3 inflammasome activation drives tau pathology. *Nature* **575**, 669–673 (2019).
43. M.-S. Tan, J.-T. Yu, T. Jiang, X.-C. Zhu, L. Tan, The NLRP3 inflammasome in Alzheimer's disease. *Mol. Neurobiol.* **48**, 875–882 (2013).
44. J. Yin, F. Zhao, J. E. Chojnacki, J. Fulp, W. L. Klein, S. Zhang, X. Zhu, NLRP3 inflammasome inhibitor ameliorates amyloid pathology in a mouse model of Alzheimer's disease. *Mol. Neurobiol.* **55**, 1977–1987 (2018).
45. L. Liu, C. Chan, The role of inflammasome in Alzheimer's disease. *Ageing Res. Rev.* **15**, 6–15 (2014).
46. R. Gordon, E. A. Albornoz, D. C. Christie, M. R. Langley, V. Kumar, S. Mantovani, A. A. B. Robertson, M. S. Butler, D. B. Rowe, L. A. O'Neill, A. G. Kanthasamy, K. Schroder, M. A. Cooper, T. M. Woodruff, Inflammasome inhibition prevents α-synuclein pathology and dopaminergic neurodegeneration in mice. *Sci. Transl. Med.* **10**, eaah4066 (2018).
47. C. Dempsey, A. R. Araiz, K. J. Bryson, O. Finucane, C. Larkin, E. L. Mills, A. A. B. Robertson, M. A. Cooper, L. A. J. O'Neill, M. A. Lynch, Inhibiting the NLRP3 inflammasome with MCC950 promotes non-phlogistic clearance of amyloid-β and cognitive function in APP/PS1 mice. *Brain Behav. Immun.* **61**, 306–316 (2017).
48. S. Ismael, S. Nasoohi, T. Ishrat, MCC950, the selective inhibitor of nucleotide oligomerization domain-like receptor protein-3 inflammasome, protects mice against traumatic brain injury. *J. Neurotrauma* **35**, 1294–1303 (2018).
49. H. Ren, Y. Kong, Z. Liu, D. Zang, X. Yang, K. Wood, M. Li, Q. Liu, Selective NLRP3 (pyrin domain-containing protein 3) inflammasome inhibitor reduces brain injury after intracerebral hemorrhage. *Stroke* **49**, 184–192 (2018).
50. B.-Z. Shao, Q. Cao, C. Liu, Targeting NLRP3 inflammasome in the treatment of CNS diseases. *Front Mol. Neurosci.* **11**, 320 (2018).
51. J. Füllgrabe, G. Ghislat, D.-H. Cho, D. C. Rubinsztein, Transcriptional regulation of mammalian autophagy at a glance. *J. Cell Sci.* **129**, 3059–3066 (2016).
52. M. Lubas, L. M. Harder, C. Kumsta, I. Tiessen, M. Hansen, J. S. Andersen, A. H. Lund, L. B. Frankel, eIF5A is required for autophagy by mediating ATG3 translation. *EMBO Rep.* **19**, e46072 (2018).
53. M. Bordi, M. J. Berg, P. S. Mohan, C. M. Peterhoff, M. J. Alldred, S. Che, S. D. Ginsberg, R. A. Nixon, Autophagy flux in CA1 neurons of Alzheimer hippocampus: Increased induction overburdens failing lysosomes to propel neuritic dystrophy. *Autophagy* **12**, 2467–2483 (2016).
54. S. Y. Cheon, H. Kim, D. C. Rubinsztein, J. E. Lee, Autophagy, cellular aging and age-related human diseases. *Exp Neurobiol* **28**, 643–657 (2019).
55. A. M. Leidal, B. Levine, J. Debnath, Autophagy and the cell biology of age-related disease. *Nat. Cell Biol.* **20**, 1338–1348 (2018).
56. J. Brouillette, R. Caillierez, N. Zommer, C. Alves-Pires, I. Benilova, D. Blum, B. De Strooper, L. Buée, Neurotoxicity and memory deficits induced by soluble low-molecular-weight amyloid-β_{1-42} oligomers are revealed *in vivo* by using a novel animal model. *J. Neurosci.* **32**, 7852–7861 (2012).
57. A. Müller-Schiffmann, A. Herring, L. Abdel-Hafiz, A. N. Chepkova, S. Schäble, D. Wedel, A. H. C. Horn, H. Sticht, M. A. de Souza Silva, K. Gottmann, O. A. Sergeeva, J. P. Huston, K. Keyvani, C. Korth, Amyloid-β dimers in the absence of plaque pathology impair learning and synaptic plasticity. *Brain* **139**, 509–525 (2016).
58. M. Jin, N. Shepardson, T. Yang, G. Chen, D. Walsh, D. J. Selkoe, Soluble amyloid β-protein dimers isolated from Alzheimer cortex directly induce Tau hyperphosphorylation and neuritic degeneration. *Proc. Natl. Acad. Sci. U.S.A.* **108**, 5819–5824 (2011).
59. C. Balducci, M. Beeg, M. Stravalaci, A. Bastone, A. Sclip, E. Biasini, L. Tapella, L. Colombo, C. Manzoni, T. Borsello, R. Chiesa, M. Gobbi, M. Salmona, G. Forloni, Synthetic amyloid-β oligomers impair long-term memory independently of cellular prion protein. *Proc. Natl. Acad. Sci. U.S.A.* **107**, 2295–2300 (2010).
60. D. M. Walsh, I. Klyubin, J. V. Fadeeva, W. K. Cullen, R. Anwyl, M. S. Wolfe, M. J. Rowan, D. J. Selkoe, Naturally secreted oligomers of amyloid β protein potently inhibit hippocampal long-term potentiation *in vivo*. *Nature* **416**, 535–539 (2002).
61. B. Parajuli, Y. Sonobe, H. Horiuchi, H. Takeuchi, T. Mizuno, A. Suzumura, Oligomeric amyloid β induces IL-1β processing via production of ROS: Implication in Alzheimer's disease. *Cell Death Dis.* **4**, e975 (2013).
62. S. Gingras, L. R. Earls, S. Howell, R. J. Smeyne, S. S. Zakharenko, S. Pelletier, SCYL2 protects CA3 pyramidal neurons from excitotoxicity during functional maturation of the mouse hippocampus. *J. Neurosci.* **35**, 10510–10522 (2015).

Acknowledgments

Funding: Research reported in this publication was supported by the National Institute of Allergy and Infectious Disease, the National Institute of Mental Health, and the National Institute on Deafness and other Communication Disorders of the NIH under award numbers R01AI40646 and R35CA231620 to D.R.G., F32AI138492 and LRPCA231423 to B.L.H., and R01MH097742 and R01DC012833 to S.S.Z.; ALSAC to D.R.G., B.L.H., and S.S.Z.; and the John H. Sununu Endowed Fellowship to B.L.H.; an EMBO Long-Term Fellowship (ALTF 1526-2016) to E.B.-R.; the Biotechnology and Biological Sciences Research Council (BBSRC) grant BB/R00904X/1 to S.C., U.M., and T.W.; and through the BBSRC Institute Strategic Programme Gut Microbes and Health BB/R012490/1: BBS/E/F/000PR10353 and BBS/E/F/000PR10355. The content herein is solely the responsibility of the authors and does not necessarily represent the official views of the NIH. **Author contributions:** B.L.H. and D.R.G. designed the experiments. B.L.H. performed and analyzed the experiments. B.J.W.T., E.B.-R., P.F., B.T., C.G., and S.S.Z. provided resources and performed and analyzed specific experiments. Mice were

generated by U.M., S.C., and T.W. to test the role played by the WD domain of Atg16L1 during aging. B.L.H. and D.R.G. wrote and edited the manuscript. **Competing interests:** B.L.H., T.W., and D.R.G. are coinventors on U.S. patent applications 62/795,217 filed 22 January 2019 and 62/797,564 filed 28 January 2019 and a worldwide patent application PCT/IB2020/050504 filed 22 January 2020 through the U.S. Patent and Trademark Office, which are currently under review. All applications are related to the work contained herein. D.R.G. consults for Ventus Therapeutics and Inzen Therapeutics. The other authors declare that they have no other competing interests. **Data and materials availability:** All data needed to evaluate the conclusions in the paper are present in the paper and/or the Supplementary Materials. Additional data related to this paper may be requested from the authors. The Atg16L1 WD domain–deficient mice can be provided by T.W. or D.R.G. pending scientific review and a completed material transfer agreement.

Submitted 26 March 2020
Accepted 2 July 2020
Published 14 August 2020
10.1126/sciadv.abb9036

Citation: B. L. Heckmann, B. J. W. Teubner, E. Boada-Romero, B. Tummers, C. Guy, P. Fitzgerald, U. Mayer, S. Carding, S. S. Zakharenko, T. Wileman, D. R. Green, Noncanonical function of an autophagy protein prevents spontaneous Alzheimer's disease. *Sci. Adv.* **6**, eabb9036 (2020).

Science Advances

Noncanonical function of an autophagy protein prevents spontaneous Alzheimer's disease

Bradlee L. Heckmann, Brett J. W. Teubner, Emilio Boada-Romero, Bart Tummers, Clifford Guy, Patrick Fitzgerald, Ulrike Mayer, Simon Carding, Stanislav S. Zakharenko, Thomas Wileman and Douglas R. Green

Sci Adv **6** (33), eabb9036.
DOI: 10.1126/sciadv.abb9036

Science Advances (ISSN 2375-2548) is published by the American Association for the Advancement of Science, 1200 New York Avenue NW, Washington, DC 20005. The title *Science Advances* is a registered trademark of AAAS.